



Since January 2020 Elsevier has created a COVID-19 resource centre with free information in English and Mandarin on the novel coronavirus COVID-19. The COVID-19 resource centre is hosted on Elsevier Connect, the company's public news and information website.

Elsevier hereby grants permission to make all its COVID-19-related research that is available on the COVID-19 resource centre - including this research content - immediately available in PubMed Central and other publicly funded repositories, such as the WHO COVID database with rights for unrestricted research re-use and analyses in any form or by any means with acknowledgement of the original source. These permissions are granted for free by Elsevier for as long as the COVID-19 resource centre remains active.



Test for Covid-19 seasonality and the risk of second waves

Francois A. Engelbrecht^{a,b,*}, Robert J. Scholes^{a,b}

^a Global Change Institute, University of the Witwatersrand, South Africa

^b Covid-19 Environmental Reference Group, South Africa

ABSTRACT

Ten months into the Covid-19 pandemic it remains unclear whether transmission of SARS-CoV-2 is affected by climate factors. Using a dynamic epidemiological model with Covid-19 climate sensitivity in the likely range, we demonstrate why attempts to detect a climate signal in Covid-19 have thus far been inconclusive. Then we formulate a novel methodology based on susceptible-infected time trajectories that can be used to test for seasonal climate sensitivity in observed Covid-19 infection data. We show that if the disease *does* have a substantial seasonal dependence, and herd immunity is not established during the first peak season of the outbreak (or a vaccine does not become available), there is likely to be a seasonality-sensitive second wave of infections about one year after the initial outbreak. In regions where non-pharmaceutical control has contained the disease in the first year of outbreak and thus kept a large portion of the population susceptible, the second wave may be substantially larger in amplitude than the first if control measures are relaxed. This is simply because it develops under the favorable conditions of a full autumn to winter period and from a larger pool of infected individuals.

1. Introduction

It is plausible that SARS-CoV-2 transmissibility depends on climatic effects, similar to the commonly circulating human coronaviruses [1–4] and influenza [5,6]. The seasonal dependence of viral respiratory diseases has been attributed to several potential mechanisms, including virus longevity in the air and on surfaces [7,8], increased susceptibility of the human victim in cold and dry weather [9,10] and changes in human social behavior between winter and summer [11].

The initial Covid-19 outbreak in December 2019 occurred in mid-latitude Northern Hemisphere countries during the boreal winter. It has since become clear that warm and humid weather has not substantially slowed down infection rates during the Northern Hemisphere summer [12], presumably because of the effects of high susceptibility of the population in the pandemic phase of the disease overwhelming any potential climatic impacts on transmissibility [2]. The disease reached the Southern Hemisphere during the austral late summer to early autumn. In the developing Southern Hemisphere countries of South America and South Africa, socio-economic factors placed limitations on the extent and duration of non-pharmaceutical control measures. Consequently, large outbreaks occurred in the winter of 2020, but with little evidence that winter climate worsened these outbreaks [13]. It remains of considerable interest, however, to understand whether Covid-19 has a seasonality dependence. A seasonal effect is potentially an important contributor to the occurrence of a second wave of outbreaks. Moreover, will Covid-19 become an annual occurrence, like

many other viral respiratory diseases?

Several studies to date have attempted to identify and quantify climatic dependencies in Covid-19 infection rates, using data on reported cases [14–17], but have failed to conclusively prove or disprove the existence of such a link. These studies have been compromised by the fact that no single location on Earth has yet moved through a full annual cycle in the presence of Covid-19; thus the studies depend on ‘space-for-time’ substitution (in other words, using the difference in climate between different locations as a proxy for its evolution over time in one location) – but the assumptions necessary for this approach to work are confounded by the spatial dynamic of the disease spread. Moreover, various degrees of non-pharmaceutical control measures have been applied across different countries, and their intensity changed over time at a given location. This, in combination with differential socio-economic conditions and related differential abilities of individuals to apply social distancing, makes it hard to identify a relatively weak climatic signal in observed case data. Further noise is added by the heterogeneity in how the case data and mortality data are reported. As a consequence of all these complicating factors, by September 2020, no consensus has been reached on whether Covid-19 has a climatic dependence; and if so, which environmental factors are involved, and what their relative strengths are [13,18].

Here we make use of a dynamic epidemiological model to identify the ‘signature’ of seasonality in the outbreak of a highly infectious disease such as Covid-19. This allows us to propose a new approach of how this signature may be detected in observed case data. We then analyse

* Corresponding author at: Global Change Institute, University of the Witwatersrand, South Africa.

E-mail address: Francois.Engelbrecht@wits.ac.za (F.A. Engelbrecht).

the conditions under which Covid-19 may resurge as a second wave of infections, and how this relates to seasonality.

2. Methods

Idealized profiles of seasonality provide a standard approach in modelling infectious diseases with seasonal behavior [3,19,20]. Following this approach, we define a ‘Theoretical Climate Correction Factor’ (TCCF) that describes how seasonality may modify the basic reproduction number R_0 :

$$TCCF = \left(\frac{1}{1+\varepsilon} \right) (1 + \varepsilon \cos(2\pi(t - \theta))) \tag{1}$$

Here ε ranges from 0 to 1 and represents the strength of seasonality, with transmissibility reaching a peak when $t = \theta$. That is, in this paper the basic reproduction number R_0 is the expected number of secondary infectious cases generated by an average infectious case in an entirely

susceptible population under climatological conditions optimal for transmission. Consistently, $0 \leq \left(\frac{1-\varepsilon}{1+\varepsilon} \right) \leq TCCF \leq 1$ and $0 \leq R_0' \leq R_0$, where R_0' is the modified reproduction number ($R_0' = TCCF * R_0$).

The TCCF can be explored over the full ranges of amplitude and timing, but here we are interested in the more limited expression of seasonality observed for the commonly circulating human coronaviruses (assuming similar behavior for SARS-CoV-2). Two recent epidemiological modelling studies have considered the degree to which seasonality may impact on the annual cycles of commonly circulating human coronaviruses. For four commonly circulating coronaviruses in Sweden, with seasonality described by an equation equivalent to (1), it was concluded that for local spread $\varepsilon = 0.15$ but for strong import of cases $0.3 \leq \varepsilon \leq 0.7$ explains the observations [3]. Using climatic dependent inverse modelling applied to case data of the HCoV-HKU1 and HCoV-OC43 coronaviruses, Fig. 1 of [2] suggests $\varepsilon \approx 0.25$ for HCoV-HKU1 and $\varepsilon \approx 0.1$ for HCoV-OC43. Consistent with these estimates and

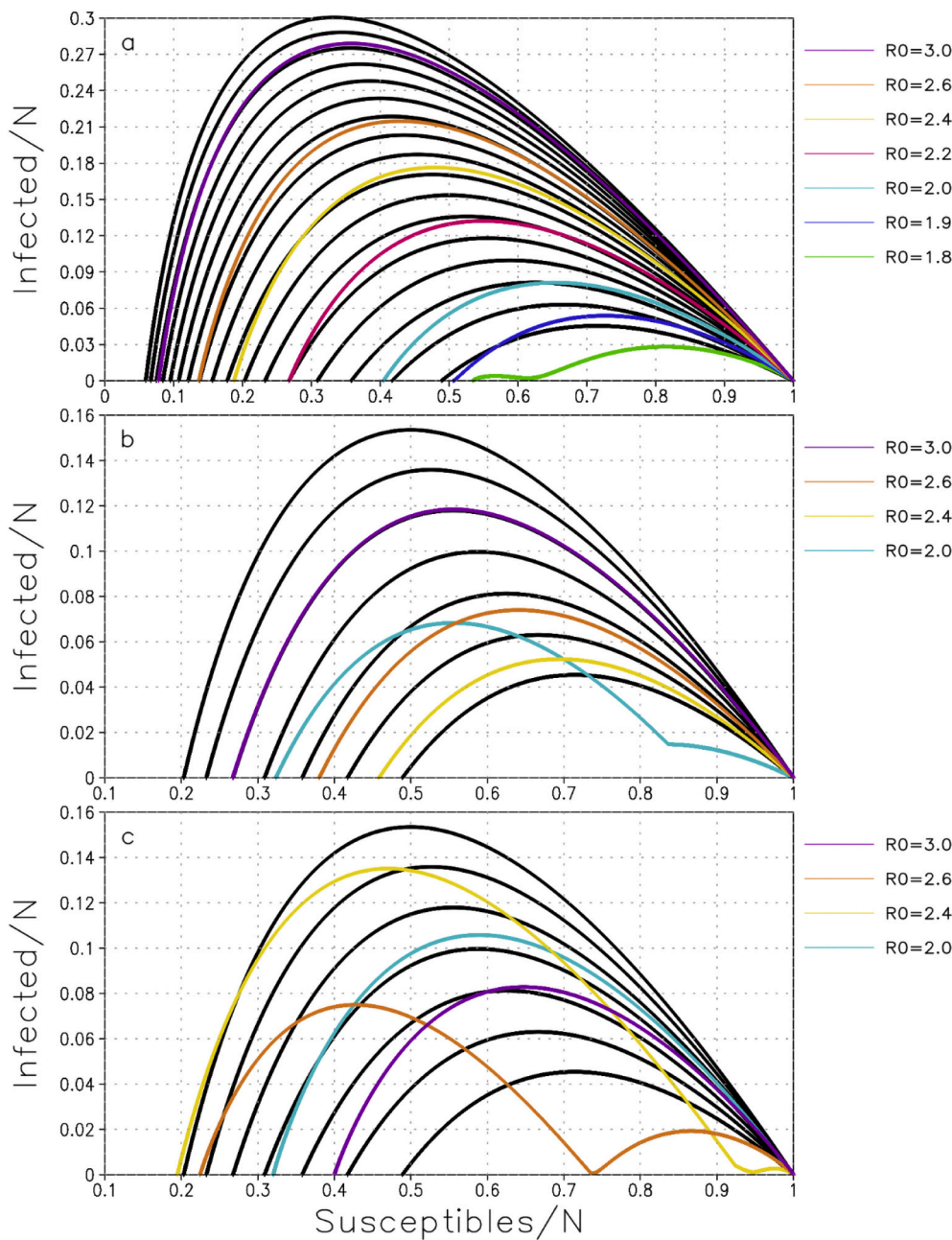


Fig. 1. Susceptible-Infected (SI) orbits for various scenarios of non-pharmaceutical control measures and seasonality of $\varepsilon = 0.2$, for the case of mid-winter onset of an infectious disease. The orbits in black represent the scenario of no control with range and R_0 interval [1.4, 3; 0.1] in a) and [1.4, 2; 0.1] in b) and c). Note the different range of I/N in a) compared to b) and c). The colored lines orbits represent a) effects of seasonality for the scenario of no control; b) effects of a lockdown followed by social distancing and c) effects of lockdown followed by social distancing in combination with seasonality. (For interpretation of the references to colour in this figure legend, the reader is referred to the web version of this article.)

restricted travel associated with the non-pharmaceutical control of Covid-19, we proceed to explore the impacts of seasonality of strength $\varepsilon = 0.2$.

We explore the signatures of seasonality in Covid-19 infection rates using a dynamic epidemiological model for the cases of mid-winter and mid-summer outbreak of the disease. In the paper, ‘mid-winter’ means 1 July (1 January) in the Southern (Northern) Hemisphere, and ‘mid-summer’ means 1 January (1 July) in the Southern (Northern) Hemisphere. For the case of (1), ‘mid-winter’ corresponds to the time during which the function attains its maximum value, and mid-summer to the time it reaches a minimum value. This is consistent with the main Covid-19 seasonality hypothesis, namely that transmissibility is favored by dry and cold winters, and reduced during warm and humid summers [21,22].

Towards identifying the key signatures of seasonality in disease propagation dynamics, we purposefully select a simple Susceptible-Infectious-Recovered-Dead (SIRD) model and apply it to a homogeneous population:

$$\begin{aligned} \frac{dS}{dt} &= -\frac{\alpha}{N}SI; \\ \frac{dI}{dt} &= \frac{\alpha}{N}SI - \beta I - \gamma I \\ \frac{dR}{dt} &= \beta I; \\ \frac{dD}{dt} &= \gamma I. \end{aligned} \quad (2)$$

Here S , I , R and D are the number of susceptible, infected, recovered and dead individuals, respectively, at a given moment in time, and they sum to the total population, N (which is assumed to remain constant). α is the daily infection rate, γ the mortality rate and β the recovery rate. Note that $R_0 = \alpha/(\gamma + \beta)$ and that the infection fatality rate (IFR) is given by $IFR = \gamma/\beta$. In the applications of the SIRD model described in this paper, α is specified to generate values of R_0 ranging between 2 and 3, in the plausible estimated range of R_0 for Covid-19 [23,24]. The values of γ and β are fixed in all the simulations at $\gamma = 0.0005 \text{ d}^{-1}$ and $\beta = 0.16 \text{ d}^{-1}$ respectively, following [25], and consistent with current estimates of the recovery rate and IFR [2,24]. Seasonality and non-pharmaceutical control measures are both modelled to impact on R_0 through changes in α .

The time it takes for an infectious disease to propagate through a population depends on its size. In the experiments performed here, $N = 15\,000\,000$. We seek to identify signatures of seasonality under the simplifying assumption of a homogeneous population, but note that in reality populations are heterogeneous and that factors such as differential population density as well as age and activity structures can impact on disease propagation dynamics [23]. The cases of non-pharmaceutical control we consider are simple and largely constant over time, but in reality such measures may be applied intermittently [26], resulting in infection curves more complex than having the single or bimodal peaks that result from the assumptions we apply. We further assume that the entire population is susceptible at the time of onset of the disease with the sole focus of exploring seasonality impacts, and not considering the potentially important role of cross-immunity that may exist in populations due to exposure to other coronaviruses [27] or potential cross-protection from for example BCG vaccination programmes [28]. Moreover, we do not distinguish between the symptomatic or asymptomatic infected and it is assumed that members from the population that recover from the disease have immunity for at least two years. The simulations do not take into account any pharmaceutical control measures that may become available in the future.

3. Results

3.1. Outbreak in mid-winter

The first case we explore is mid-winter onset of the disease in the presence of seasonality described by $\varepsilon = 0.2$ under (1). The susceptible-infected (SI) orbits (time trajectories in the SI phase-plane, shown as proportions of the total population, N) for different values of R_0 for the scenario of ‘no control measures and no seasonality effects’ are shown in black in Fig. 1a, b and c. The orbits commence with effectively an entirely susceptible population ($S = N - 1$, $I = 1$) and then follow a hump-shaped trajectory, with the peak infection also being the point where a sufficient number of people have been infected for herd immunity to set in. The point where the orbit returns to the S-axis represents the final epidemic size. The effect of seasonality, in the absence of control measures, is explored in Fig. 1a for several values of R_0 (colored orbits), while the effect of non-pharmaceutical control [29] without seasonality effects is shown in Fig. 1b (colored orbits). For the non-pharmaceutical control scenarios it is assumed that after a period of one month of the disease spreading in the population, a lockdown is implemented which reduces the infection rate by 40% (i.e. $R_0' = 0.6R_0$). The lockdown is maintained for 9 months, through spring, summer and into autumn, followed by light social distancing (i.e. a 10% reduction in infection rate). The final scenario considered applies the same non-pharmaceutical control measures whilst seasonality is also having an effect (Fig. 1c, colored orbits). The corresponding time-evolution of the fraction of the population infected (I/N) is shown in Fig. 2a to d for selected values of R_0 , for the scenarios of no control measures and no seasonality (black lines), no control measures in the presence of seasonality (green lines), lockdown followed by social distancing in the absence of seasonality (yellow lines) and finally, lockdown followed by social distancing, both in the presence of seasonality effects (red lines).

In the initial stages of a mid-winter onset the disease with no control measures being applied, $R_0' \approx R_0$ ($TCCF \approx 1$). As winter progresses to spring, progressively warmer and more humid conditions reduce R_0' . The telltale signature of such an effect is that the SI-orbits under seasonality (colored lines in Fig. 1a) cross the orbits for the scenario of no control and no seasonality. This effect can be seen in in Fig. 1a, most prominently for the lower values of R_0 ($R_0 \leq 2$), but also at higher values ($R_0 = 2.2, 2.4, 2.6$) once about 50% of the population has been infected. At lower infection rates, the disease takes relatively long to spread through the population, pushing it into spring and allowing seasonality to lower R_0' . For example, for $R_0 = 2$ in the absence of seasonality the peak infection occurs in spring, 3.5 months into the outbreak (Fig. 2d, black line). If seasonal effects are at work, the peak infection is reached about two weeks later - but most importantly, the peak of active cases, which is what determines the load on the health system, is almost halved (Fig. 2d, green line). The resulting behavior of the disease, in terms of the total fraction of the population eventually infected, resembles that of an infection with constant $R_0 = 1.5$ (Fig. 1a). By the time that the disease has run its course and the final epidemic size is reached, less than 60% of the population has been infected, while over 80% of the population is infected if seasonality is not at work. In contrast, if the basic reproduction number is at the high end ($R_0 = 3$), the peak infection in the absence of seasonality occurs less than 2 months after introduction of the first infected individual to the population (Fig. 2a, black line). Even if seasonality effects are considered, given that climatological effects are optimal for transmission for the case of mid-winter outbreak, there is not enough time for seasonality to impact the infection rate (Fig. 2a, green line).

Non-pharmaceutical control slows down the spread of the disease, but if maintained consistently for a sufficiently long period, it should still be possible to discern signatures of seasonality from the SI-orbits. This is explored in Fig. 1b and c. Note that the range of both the S- and I-axes have been reduced compared to Fig. 1a and that only a subset of orbits are shown to avoid clutter. For the illustrated scenario, a strong

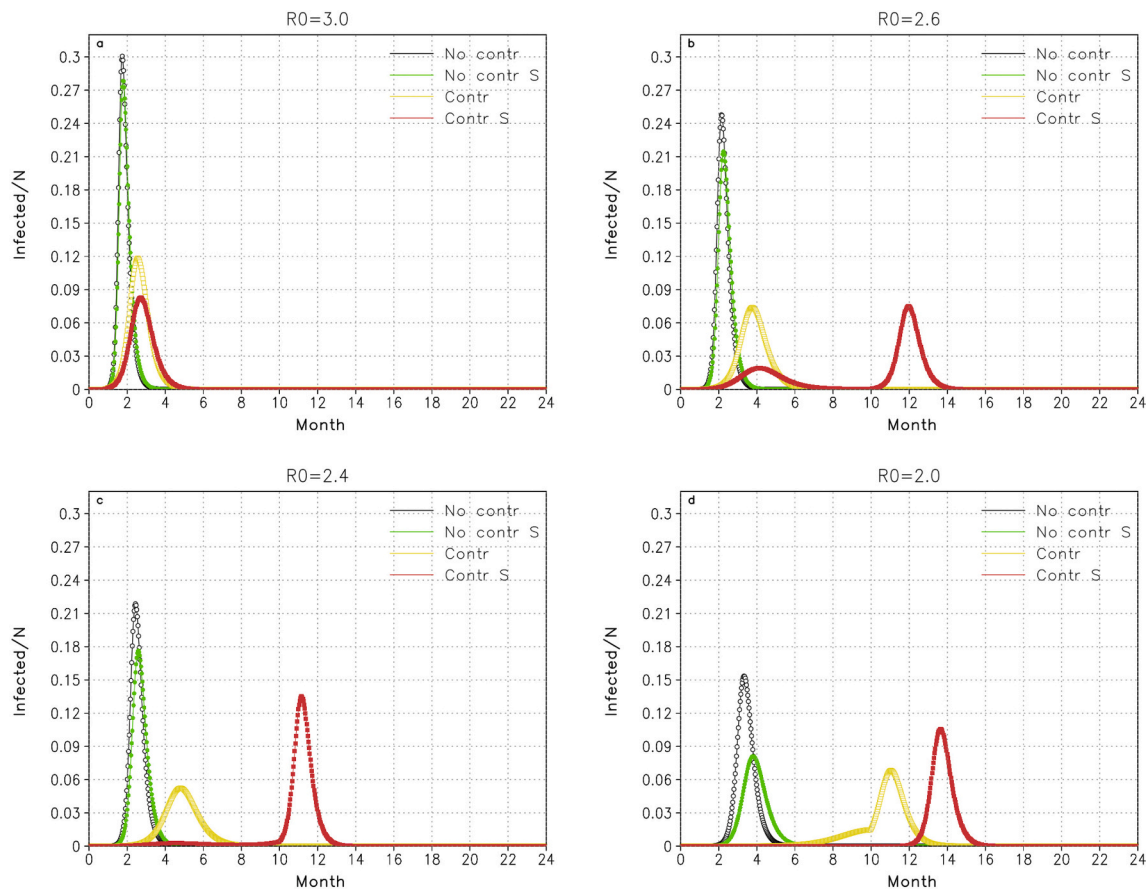


Fig. 2. Evolution of I/N for an infectious disease for different values of R_0 and where onset occurs in mid-winter. The black lines represents the scenario of no control measures and no seasonality, the green lines represent no control measures but with seasonality effects included, the yellow lines represent non-pharmaceutical control measures (see the text for details) and the red lines indicate the effects of seasonality in combination with non-pharmaceutical control. Seasonality is for $\epsilon = 0.2$. (For interpretation of the references to colour in this figure legend, the reader is referred to the web version of this article.)

lockdown was initiated one month after onset of the disease and maintained for 9 months, where after it was replaced by social distancing. The SI-orbits display two main types of behavior. For values of $R_0 \geq 2.2$, although the infection rate is significantly damped, the disease still spreads through most of the population and peak infection occurs within six months of the outbreak (Fig. 2 a to c, yellow lines). In these cases 50–75% of the population become infected before the final epidemic size is reached (Fig. 1b). For lower basic reproduction numbers (e.g. $R_0 = 2$) the dampening of the infection rate by control measures is sufficiently strong that no significant outbreak occurs during the 9 month period of lockdown (see the blue line representing $R_0 = 2$ in Fig. 1b and the yellow line up and until month 10 in Fig. 2d). However, since herd immunity is not reached, the disease continues to linger in the population, and breaks out in the months immediately following the relaxation of lockdown measures (Fig. 1b blue orbit, Fig. 2d, yellow line beyond month 10). In terms of the SI-orbits, the outbreak can be seen as a sudden increase in R_0' and the consequent crossing of the orbits of constant R_0 .

The presence of seasonality implies further dampening of infection rates during the period of stringent lockdown. For $R_0 = 3$ the characteristic signature of seasonality, namely the crossing of the orbits of constant R_0 is apparent (compare the purple orbits in Fig. 1b and c), but despite the combined dampening effects of lockdown and seasonality the diseases still propagates through the population until herd immunity is reached in spring (Fig. 2a, red line) with about 60% of the population infected during the course of the outbreak (purple orbit, Fig. 1c). The remaining cases ($R_0 \leq 2.6$) displayed in Fig. 1c reveal an entirely different type of behavior, induced by seasonality. For these lower

infection rates the combined dampening effect of lockdown and seasonality is sufficiently strong that the peak infection is substantially reduced (Fig. 2 b to d) and less than 25% of the population becomes infected during the period of stringent lockdown (Fig. 1c). High summer temperatures following the initial onset of the disease further damp the infection rate, but since herd immunity is not attained, once lockdown is replaced by less stringent social distancing, the return of lower temperatures and humidity as the next winter approaches systematically increases the infection rate. Without renewed lockdown, this results in a second wave of outbreak, with a significantly higher of peak infection than experienced in the first year of the disease (red lines in Fig. 2 b to d). This scenario may well be important for Northern Hemisphere countries, where initial onset of the disease occurred in approximately mid-winter, and where anti-body tests suggest that the portion of the population infected by mid-summer is significantly less than 20% [30].

3.2. Outbreak in mid-summer

The impacts of seasonality as described by (1) for $\epsilon = 0.2$ are profoundly different for a mid-summer onset compared to mid-winter onset of the disease, under the scenario of no control measures being applied. The SI-orbits for the case of a mid-summer outbreak are shown in Fig. 3a to c under scenarios of non-pharmaceutical control and seasonality effects, with the corresponding I/N time-evolutions shown in Fig. 4. The summer season substantially dampens the infection rate ($T_{CF} \approx 0.7$) and consequently delays the peak infection by about a month for $R_0 = 3$ (Fig. 4a, green line) and two months for $R_0 = 2$ (Fig. 4d, green line). For larger values of R_0 peak infection occurs before optimal seasonality

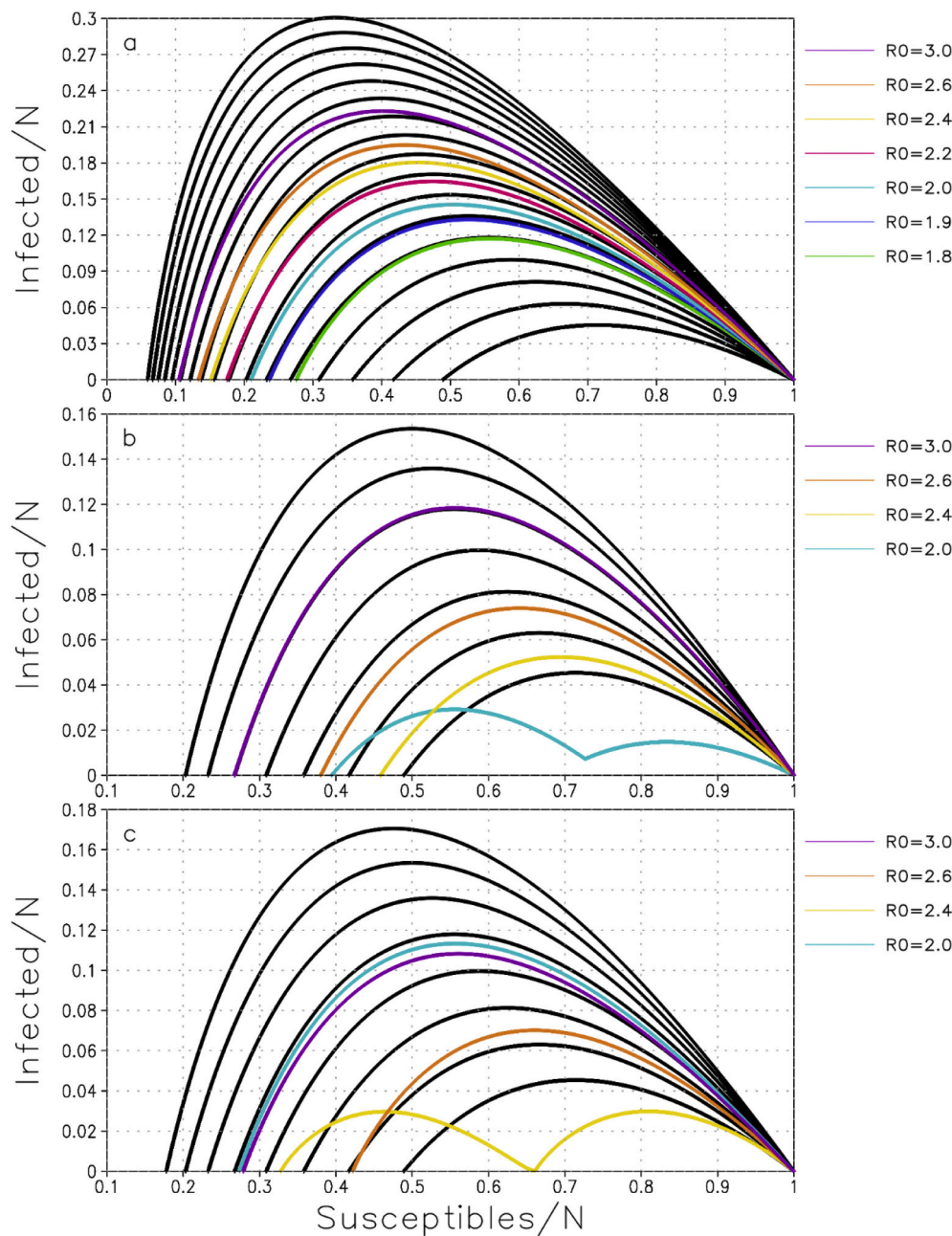


Fig. 3. Susceptible-Infected (SI) orbits for various scenarios of non-pharmaceutical control measures and seasonality of $\epsilon = 0.2$, for the case of mid-summer onset of an infectious disease. The orbits in black represent the scenario of no control with range and R_0 interval $[1.4, 3; 0.1]$ in a) and $[1.4, 2; 0.1]$ in b) and c). Note the different range of I/N in a) compared to b) and c). The colored lines orbits represent a) effects of seasonality for the scenario of no control; b) effects of a lockdown followed by social distancing and c) effects of lockdown followed by social distancing in combination with seasonality. (For interpretation of the references to colour in this figure legend, the reader is referred to the web version of this article.)

forcing is reached in winter. By the time of peak infection (early autumn for $R_0 = 3$ to late autumn for $R_0 = 2.4$), R_0' has increased sufficiently for the orbits of constant R_0 to be crossed (see the colored orbits in Fig. 3a). The dampening of the peak infection by seasonality is substantial, even for these higher values of R_0 . For example, for $R_0 = 3$ the dampening of the peak infection is about 40% (Fig. 4a) and 10% less of the population is infected by the time the final epidemic size is reached (Fig. 3a). For $R_0 \leq 2$ the damping is so significant that the outbreak only gains momentum in the following winter, reaching the same peak infection (Fig. 4d, green line) and infecting the same portion of the population (Fig. 3c) as for the corresponding situation of no control measures and no seasonality (Fig. 4d, black line).

We next explore a scenario of non-pharmaceutical control similar to that described for the mid-winter onset, but with lockdown maintained from the end of month one to the end of month 12. For values of $R_0 \gg 2.2$ even under a stringent lockdown, the disease still runs its course through the population and herd immunity is reached during the first year of the

infection (Fig. 3b). The same will thus be true for all weaker forms of lockdown and social distancing. Nonetheless, the amplitude of the peak infection is substantially reduced and its timing is delayed (Fig. 4a to c, yellow lines). The lockdown orbits correspond to cases of constant R_0 given that the lockdown merely functions to reduce R_0 to a smaller but constant value of R_0' . For values of $R_0 \leq 2$ the dampening of the infection rate is so strong that herd immunity is not reached during the first year of the infection (blue orbit, Fig. 3b). Once the measures of control are relaxed in the 13th month of the infection, a second wave of infections occurs immediately (blue orbit, Fig. 3b; yellow line, Fig. 4d).

For a mid-summer onset, seasonality combined with non-pharmaceutical controls dampen the infection rate during the initial months of the outbreak, but when winter arrives the transmission-reducing effect of seasonality disappears. Consequently, a peak infection of amplitude similar to the case of lockdown without seasonality effects occurs for values of $R_0 \geq 2.6$; (Fig. 4a and b). This is demonstrated best for the case of $R_0 = 2.6$ in Fig. 3c (orange orbit), where R_0' first

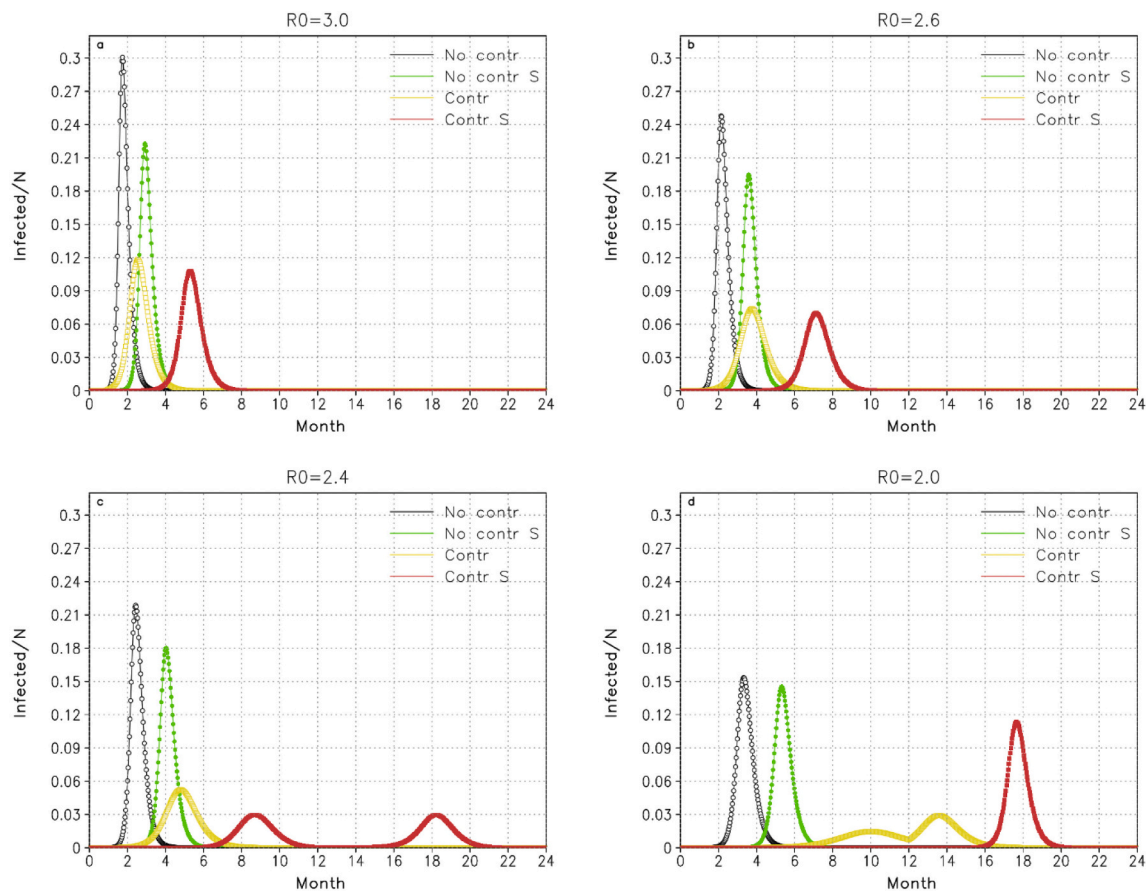


Fig. 4. Evolution of I/N for an infectious disease for different values of R_0 and where onset occurs in mid-summer. The black lines represents the scenario of no control measures and no seasonality, the green lines represent no control measures but with seasonality effects included, the yellow lines represent non-pharmaceutical control measures (see the text for details) and the red lines indicate the effects of seasonality in combination with non-pharmaceutical control. Seasonality is for $\epsilon = 0.2$. (For interpretation of the references to colour in this figure legend, the reader is referred to the web version of this article.)

increases as winter is reached, where after it decreases as the disease runs its course in spring, with a clear crossing of the orbits of constant R_0 . For smaller values of R_0 , herd immunity is not reached during the first year of infection, thus once control measures are weakened second waves of infection follow (blue and yellow orbits in Fig. 3c; red lines in Fig. 4c and d). These do not occur immediately, as is the case in the absence of seasonality. Rather, the infection rate remains damped by seasonality in the summer and autumn of the second year of the disease, and peak infection only occurs in the winter or spring of the second year. For $R_0 = 2$ most of the population is still susceptible after the first year of the infection (blue orbit, Fig. 3c), and consequently the second wave of infections can be severe (in the absence of control measures being re-applied in the second year of the infection (red line, Fig. 4d).

4. Discussion

By late September 2020, ten months into the Covid-19 outbreak, it remains unclear whether transmission of SARS-CoV-2 is impacted by climatic effects [12,18]. A key reason for this is that the majority of studies exploring climate effects focused on the initial outbreak of the disease before non-pharmaceutical control measures impacted on infection rates. These studies thus focused on relatively short periods and relied on a ‘space-for-time’ substitution to incorporate a greater variety of climate anomalies, but at the expense of introducing several confounding factors to the analysis. Here we propose an alternative methodology to test for Covid-19 seasonality. This methodology considers the evolution of Covid-19 over longer periods of time, including at least one winter/summer and one transition (spring/autumn) season, to

explore the systematic impacts of seasonality rather than the instantaneous impacts of climate anomalies on infection rates. Moreover, unlike previous studies the methodology considers the full dynamics of the disease through considering its SI-orbits, rather than to focus on infection rates only. We’ve used a SIRD modelling approach to explore the signatures of seasonality of a highly infectious disease under the proposed methodology, also considering the confounding impacts of non-pharmaceutical control. We consider idealized cases of mid-summer and mid-winter outbreaks, noting the current hypothesis that Covid-19 infection rates are optimal under cold and dry conditions. In such climates, the telltale signature of seasonality is the crossing of the SI-orbits of constant R_0 by the seasonality orbits on an SI-diagram, which can be detected even in the pandemic stage of the outbreak.

In the case of mid-winter onset, without control measures, the detectability of even strong seasonality only becomes feasible for $R_0 > 2$ once about 50% of the population has been infected. For lower values of R_0 , the disease persists in the population for long enough for seasonality to be more clearly revealed. Control measures slow down the progression of the disease, but if applied consistently for many months the presence of seasonality can be clearly detected in the SI orbits. However, stringent lockdown measures prevent the development of herd immunity so that more than 70% of the population remain susceptible in the summer following the initial onset of the disease. Should control measures be relaxed in summer due to either a false sense of security that the disease has been contained, or under socio-economic pressure, severe seasonality-induced second waves can develop from autumn to spring of the following year. It may be noted that current serological testing in several Northern Hemisphere countries where Covid-19 had a winter

onset is suggesting that significantly less than 20% of the population had been infected by the time of the onset of the boreal summer of 2020 [30].

When the disease onset occurs in mid-summer its evolution is markedly different. Despite the dampening effects of climate, the disease still moves through the population for values of $R_0 > 2$ and herd immunity is reached before winter arrives. The seasonality-affected orbits cross the orbits of constant R_0 only by the time that about half of the population has been infected. For lower values of R_0 the disease is still propagating through the population by the time winter arrives and it reaches its full transmission probability, thus peak infection is similar to that in the absence of seasonality effects, with the seasonal orbits tangential to those of constant R_0 . For high values of R_0 ($R_0 \geq 2.6$) stringent control measures, even in combination with seasonal dampening, merely function to slow down the propagation of the disease and herd immunity is reached in the first year of the outbreak. For lower values of R_0 , the effect of lockdown and seasonal dampening is so substantial that herd immunity is not achieved in the first year of outbreak, and in the presence second waves of high peak infection occur in the second year when winter sets in (and provided control measures have been relaxed). Given the timing of the Covid-19 outbreak, this risk applies to Southern Hemisphere countries such as Australia and New Zealand, where efficient non-pharmaceutical control measures are on track to prevent herd immunity from being reached in 2020.

The telltale signature of seasonality is that the seasonal orbits cross those of a constant R_0 . The identification of this feature in real-world data, if it exists, will be confounded by inadequacies and differences in how infection rates are reported between countries. This problem may be reduced by using death-rate anomalies (excess deaths) as a proxy for Covid-19 mortality rates, from which inverse modelling may be applied to construct the SI-orbits. A further complicating factor is the temporally-varying application of non-pharmaceutical control measures. Nonetheless, we are of the view that the proposed test for seasonality can be successfully applied to a subset of countries, regions or cities, where non-pharmaceutical control measures have been applied consistently for several months. Still, about half of the population needs to become infected for the seasonality feature to clearly develop, further limiting the subset of populations within which a seasonality signature can likely be detected (as by September 2020). Given the limitations of operational Covid-19 statistics, the less than full annual cycle for which Covid-19 has been spreading on the planet and the fact that in most countries only a relatively small portion of the population has to date been infected, it is not surprising that no consensus has so far been reached in terms of seasonality impacts on Covid-19. The signal is obscured by both the noise of inconsistent data reporting, but also by the fundamental properties of the disease.

By September 2020 the main immediate application of clearer knowledge of Covid-19 seasonality is preparation for, or prevention of, seasonality-induced second waves of infection (the ultimate signature of seasonality). This risk is particularly large in the absence of widespread deployment of a vaccine and in countries where successful non-pharmaceutical control have let a large portion of the population susceptible after the initial outbreak. Until the importance of seasonality in Covid-19 infection rates has been established, it remains prudent to design control measures as if high temperature and humidity will *not* significantly dampen the infection rate [12,18]. At the same time, however, it is important to design control measures to cater for the possibility of severe, seasonality-induced second waves of infection.

Declaration of Competing Interest

None.

References

- [1] E.R. Gaunt, A. Hardie, E.C. Claas, P. Simmonds, K.E. Templeton, Epidemiology and clinical presentations of the four human coronaviruses 229E, HKU1, NL63, and OC43 detected over 3 years using a novel multiplex real-time PCR method, *J. Clin. Microbiol.* 48 (2010) 2940–2947.
- [2] R.E. Baker, W. Yang, G.A. Vecchi, C.J.E. Metcalf, B.T. Grenfell, Susceptible supply limits the role of climate in the early SARS-CoV-2 pandemic, *Science* (2020), <https://doi.org/10.1126/science.abc2535>.
- [3] R.A. Neher, R. Dyrdak, V. Druelle, E.B. Hodcroft, J.A. Albert, Potential impact of seasonal forcing on a SARS-CoV-2 pandemic, *Swiss Med. Wkly.* 50 (2020) w20224, <https://doi.org/10.4414/smww.2020.20224>.
- [4] S. Nickbakhsh, A. Ho, D.F.P. Marques, J. McMenamin, R.N. Gunson, P.R. Murcia, Epidemiology of seasonal coronaviruses: establishing the context for the emergence of coronavirus disease 2019, *J. Infect. Dis.* 222 (2020) 17–25.
- [5] J. Shaman, V.E. Pitzer, C. Viboud, B.T. Grenfell, M. Lipsitch, Absolute humidity and the seasonal onset of influenza in the continental United States, *PLoS Biol.* 8 (2010), e1000316, <https://doi.org/10.1371/journal.pbio.1000316> Medline.
- [6] V.N. Petrova, C.A. Russell, The evolution of seasonal influenza viruses, *Nat Rev Microbiol.* 16 (2020) 47–60, <https://doi.org/10.1038/nrmicro>.
- [7] A.C. Lowen, S. Mubareka, J. Steel, P. Palese, Influenza virus transmission is dependent on relative humidity and temperature, *PLoS Pathog.* 3 (2007) 1470–1476.
- [8] A.C. Lowen, J. Steel, S. Mubareka, P. Palese, High temp (30 °C) blocks aerosol but not contact transmission of influenza virus, *J. Virol.* 82 (2008) 5650–5652.
- [9] P.D. Shaw Stewart, Seasonality and selective trends in viral acute respiratory tract infections, *Med. Hypotheses* 86 (2016) 104–119.
- [10] E. Kudo, E. Song, L.J. Yockey, T. Rakib, P.W. Wong, R.J. Homer, A. Iwasaki, Low ambient humidity impairs barrier function and innate resistance against influenza infection, *Proc. Natl. Acad. Sci. U. S. A.* 116 (2019) 10905–10910, <https://doi.org/10.1073/pnas.1902840116>.
- [11] E. Lofgren, N.H. Fefferman, Y.N. Naumov, J. Gorski, E.N. Naumov, Influenza seasonality: underlying causes and modeling theories, *J. Virol.* 81 (2007) 5429–5436.
- [12] C.J. Carlson, A.C.R. Gomez, S. Bansal, S.J. Ryan, Misconceptions about weather and seasonality must not misguide COVID-19 response, *Nat. Commun.* 11 (2020) 4312, <https://doi.org/10.1038/s41467-020-18150-z>.
- [13] A.J. Smit, J.M. Fitchett, F.A. Engelbrecht, R.J. Scholes, G. Dzihvhuho, N.A. Sweijd, Winter is coming: a southern hemisphere perspective of the environmental drivers of SARS-CoV-2 and the potential seasonality of COVID-19, *Int. J. Environ. Res. Public Health* 17 (2020) 5634, <https://doi.org/10.3390/ijerph17165634>.
- [14] G.F. Fioleta, D. Rubolini, Climate affects global patterns of COVID-19 early outbreak dynamics, *medRxiv* (2020). DOI: 2020.03.23.20040501.
- [15] C. Merow, M.C. Urban, Seasonality and uncertainty in COVID-19 growth rates, *medRxiv* (2020), <https://doi.org/10.1101/2020.04.19.20071951>.
- [16] H. Qi, S. Xiao, R. Shi, M.P. Ward, Y. Chen, W. Tu, Q. Su, W. Wang, X. Wang, Z. Zhang, COVID-19 transmission in Mainland China is associated with temperature and humidity: A time-series analysis, *Sci. Total Environ.* 728 (2020), <https://doi.org/10.1016/j.scitotenv.2020.138778>.
- [17] M.M. Sajadi, P. Habibzadeh, A. Vintzileous, S. Shokouhi, F. Miralles-Wilhelm, A. Amoroso, Temperature, humidity, and latitude analysis to estimate potential spread and seasonality of coronavirus disease 2019 (COVID-19), *JAMA Network Open.* 3 (2020) e2011834.
- [18] K.M. O'Reilly, M. Auzenbergs, Y. Jafari, Y. Liu, S. Flasche, R. Lowe, Effective transmission across the globe: the role of climate in COVID-19 mitigation strategies, *The Lancet Planetary Health* 4 (2020), e172, [https://doi.org/10.1016/S2542-5196\(20\)30106-6](https://doi.org/10.1016/S2542-5196(20)30106-6).
- [19] J. Dushoff, J.B. Plotkin, S.A. Levin, D.J.D. Earn, Dynamical resonance can account for seasonality of influenza epidemics, *Proc. Natl. Acad. Sci. U. S. A.* 101 (2004) 16915–16916, <https://doi.org/10.1073/pnas.0407293101>.
- [20] S. Chen, B. Epaneanu, Regular biennial cycles in epidemics caused by parametric resonance, *J Theor Biol.* 415 (2020) 137–144, <https://doi.org/10.1016/j.jtbi.2016.12.013>.
- [21] Q. Bukhari, J.M. Massaro, R.B.Sr. D'Agostino, S. Khan, Effects of Weather on Coronavirus Pandemic, *Int. J. Environ. Res. Public Health* 17 (2020) 5399, <https://doi.org/10.3390/ijerph17155399>.
- [22] J. Wang, K. Tang, K. Feng, X. Lin, W. Lv, K. Chen, F. Wang, High Temperature and High Humidity Reduce the Transmission of COVID-19, SSRN: <https://ssrn.com/abstract=3551767>.
- [23] T. Britton, F. Ball, P. Trapman, A mathematical model reveals the influence of population heterogeneity on herd immunity to SARS-CoV-2, *Science* 369 (2020) 846–849.
- [24] A. Fontanet, S. Cauchemez, COVID-19 herd immunity: where are we? *Nat. Rev. Immunol.* 20 (2020) 583–584, <https://doi.org/10.1038/s41577-020-00451-5>.
- [25] C. Anastassopoulou, L. Russo, A. Tsakris, C. Siettos, Data-based analysis, modelling and forecasting of the COVID-19 outbreak, *PlosOne* (2020), <https://doi.org/10.1371/journal.pone.0230405>.
- [26] S.M. Kissler, C. Tedijanto, E. Goldstein, Y.H. Grad, M. Lipsitch, Projecting the transmission dynamics of SARS-CoV-2 through the postpandemic period, *Science* 368 (2020) 860–868.
- [27] A. Sette, S. Crotty, Pre-existing immunity to SARS-CoV-2: the knowns and unknowns, *Nat Rev Immunol* (2020), <https://doi.org/10.1038/s41577-020-0389-z>.

- [28] L.E. Escobara, A. Molina-Cruz, C. Barillas-Mury, BCG vaccine protection from severe coronavirus disease 2019 (COVID-19), *PNAS* (2020), <https://doi.org/10.1073/pnas.2008410117>.
- [29] T. Hale, S. Webster, A. Petherick, T. Phillips, B. Kira, Oxford COVID-19 Government Response Tracker, Blavatnik School of Government, 2020. <https://www.bsg.ox.ac.uk/research/research-projects/oxford-covid-19-government-response-tracker>.
- [30] M. Pollán, B. Pérez-Gómez, R. Pastor-Barriuso, J. Oteo, M.A. Hernán, M. Pérez-Olmeda, J.L. Sanmartín, A. Fernández-García, I. Cruz, N.F. de Larrea, M. Molina, F. Rodríguez-Cabrera, M. Martín, P. Merino-Amador, J.L. Paniagua, J.F. Muñoz-Montalvo, F. Blanco, R. Yotti, Prevalence of SARS-CoV-2 in Spain (ENE-COVID): a nationwide, population-based seroepidemiological study, *Lancet* (2020), [https://doi.org/10.1016/S0140-6736\(20\)31483-5](https://doi.org/10.1016/S0140-6736(20)31483-5).